Available online at www.sciencedirect.com
SCIENCE DIRECT
Journal of Power Sources 156 (2006) 85–91
JOURNAL OF POWER SOURCES
www.elsevier.com/locate/jpowsour

Fuel cell operation characterization using simulation

Pascal Schott *, Pierre Baurens

Fuel Cell Laboratory, Commissariat à l'Energie Atomique, Grenoble, France

Available online 18 October 2005

Abstract

The first step of fuel cell stack characterization consists in experimental testing of its global electrochemical performances under various working conditions. The second step is devoted to link the collected data to local species concentrations, membrane hydration and resulting current density in the stack. In the project PICOS, we have to characterize a 1.5 kW 12-cells' stack of 330 cm^2. The stack performances are measured on a specific test bench and analyzed using a fuel cell-stack modeling tool. The test bench allows to control the oxygen (or air) and hydrogen flow rates and humidity at the inlet of the stack, the pressure at the outlet, and the delivered current. Each cell potential and the total stack potential are monitored, the produced water is condensed at the outlet in order to measure its amount. The model used is a mono-dimensional description of a single cell. It is based on a semi-empirical law for the local electrochemical response computation. The local pressures, temperatures, gas compositions and membrane hydration are computed dynamically. A semi-empirical electrochemical model of the active layer is fitted to experimental data, the gas diffusion layer porosity and electro-osmosis coefficient of the membrane have been adjusted to obtain the best fit. The simulations calculate the cell potential and the current density profile in the cell for various feeding conditions. The simulations allow us to explain the effect of gas hydration on the stack potential and to predict possible drying out of the membrane.

Keywords: Fuel cell; Characterization; Simulation

1. Introduction

One of the tasks of the PICOS project is to characterize the operation of a 1.5 kW Sorapec-manufactured stack of 12 cells of 330 cm^2. The membranes are made of Nafion® 115, we have no information about the electrodes. The objective of this characterization is the evaluation of the internal temperatures, partial pressures, membrane hydration, liquid water saturation, and resulting current density distribution during operation under different experimental conditions. This task can hardly be achieved by direct measurement, because adapted sensors (for instance to measure the partial pressure of oxygen inside the electrodes) are not available, and if they are, it is not possible to insert them in an already existing and closed industrial stack. So experimental data is limited to fluids inlet and outlet conditions, global stack current and cells potentials, bipolar plates temperatures. The way to go ahead of these practical limitations is to build a model of what happens inside the cells. To be able to give some insight on the internal mechanisms, this model has to be based on physical phenomena involved in the fuel cell response.

2. Experimental aspects

The stack is tested on a specific test bench (Fig. 1) that allows to impose independently the oxygen (or air) and hydrogen flow rates, the gases' temperature and water content at the stack inlet, the gas pressure at the stack outlets and the delivered current.

The stack temperature is controlled by varying the temperature and the flow rate of de-ionized water in a separated cooling loop. Thanks to a fluid distributor inside the stack, the bipolar plates are all cooled in parallel, but the temperature can only be regulated on one plate (the one located in the middle of the stack has been chosen). Fig. 2 shows that the temperatures of the other plates (excepted end plates) are close. The potential of each cell, the total stack potential and the temperatures of each bipolar plate and end plates are monitored. The produced water is condensed and collected at the outlet and its amount is measured at the end of a operation cycle in order to estimate the water transfer across the membrane and to check the gas humidification. The water transfer across the membrane is found to

* Corresponding author.
E-mail address: pascal.schott@cea.fr (P. Schott).

0378-7753/$ – see front matter © 2005 Elsevier B.V. All rights reserved.
doi:10.1016/j.jpowsour.2005.08.034

Fig. 1. Stack mounted on the experimental test bench.

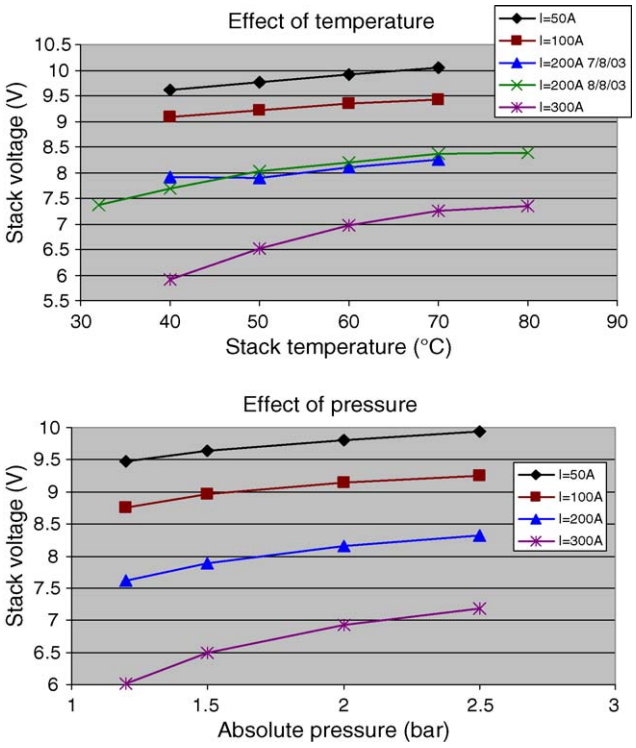

Fig. 3. Influence of the temperature and pressure on the stack voltage for different values of current.

be negligible compared to the amount of water produced during operation.

In order to fit the model (see Section 4), the steady-state stack voltage is recorded for different values of temperature and pressure (Fig. 3). In these experimental runs, the stack is fed with pure and dry oxygen and hydrogen and with stoichiometric ratios of 1.4 for oxygen and 1.05 for hydrogen. The delivered current is successively fixed to 50, 100, 200 and 300 A. Each point is hold during at least 15 min (depending on observed deviation of cell voltage in mV min^{-1}) in order to be sure of steady-state operation. No effect of gas hydration is noticed under these working conditions, the reproducibility of the tests is good and all the cells have roughly the same voltage (Fig. 2). This confirms that there is no fluid misdistribution in the stack and allows (for modeling purpose) to represent the stack by an equivalent single cell.

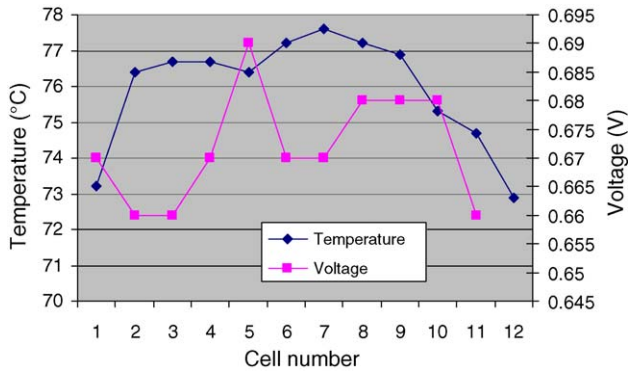

Fig. 2. Typical voltage and temperature distribution in the stack (H_2/O_2) at 200 A.

These experimental data allow to fit the model, mainly the parameters for the electrochemical response of the cell (30). In a second phase, experimental runs using air instead of pure oxygen allow us to fit the porosity of the gas diffusion layer and to observe an effect of gas hydration (Section 5).

3. Fuel cell model

Our model results of several PhD and project studies around polymer electrolyte fuel cell simulation [1,3]. The fuel cell modeling activity at CEA started about 10 years ago with a stationary model able to simulate the steady-state current–potential response of a single fuel cell [3]. This model based on [5] was improved in order to take into account two-phases flows in the gas diffusion layers and in the active layers of the electrodes. The main purpose of this work was to explain the potential drop of the cells at high current densities, giving a qualitative and quantitative answer to the question: diffusion limitation, drying out of the anode or flooding of the cathode? With growing interests for transportation applications (implying transient operation) and improvement of computing techniques, a dynamic model has been developed [1] in order to simulate non-stationary cycles [6], to test regulation strategies [7] and to be able to exploit transient experimental results for understanding global fuel cell operation. As commercial membrane-electrodes assemblies (MEA), without access to internal compositions but with high repeatability are now used, the model of active layer is simplified to a semi-empirical law fitted on experimental data [2].

3.1. General description

This semi-empirical law allows to compute the potential versus current response of the MEA given the local pressures, temperatures and species concentrations at the active layers [1,2]. These local conditions are dynamically computed using conservation and mass transport laws in the different parts of the cell (channels, gas diffusion layers, membrane). The described phenomena are: pressure drop in the gas distributors, gas diffusion in the electrodes, liquid water transport in the electrodes, water transport in the membrane, ohmic loss in the membrane, heat production and transfer. The main assumptions supporting the model are that the local electrochemical cell response time is fast (typically less than that 10^{-3} s) and that the mass and thermal transport are slow (typically from 10^{-1} to 10^{2} s), so they have to be computed dynamically in the context of transportation applications.

3.2. Gas distributors

Gas distributors (in our case channels) are 1D-meshed from the gas inlets to the gas outlets. Mass and thermal balances are computed on each mesh considering gas inlet, gas outlet, oxygen or hydrogen consumption, water production, water condensation or evaporation and heat exchanges with the bipolar plate and the gas diffusion layer. Pressure drop is modeled using simplified linear correlations (1) and (2).

$$Q_{\text{gaz}} = \frac{A(1-s)C_{\text{q}_{\text{gaz}}}}{L}\Delta P_{\text{gaz}} \tag{1}$$

$$Q_{\text{liq}} = \frac{AsC_{\text{q}_{\text{liq}}}}{L}\Delta P_{\text{liq}} \tag{2}$$

These relations are given in [8], Q is the volumic flow rate; A and L, the cross section and the length of the channel, respectively; s the fraction of volume occupied by the liquid water; C_{q} a coefficient to fit and ΔP the pressure drop. The liquid phase is represented by subscript liq, the gas phase by gaz.

3.3. Electrodes (hydraulic aspect)

The hydraulic model of electrode is decomposed into two parts, the one is computing the gas and water transport across the gas diffusion layer (GDL), the other is computing the mass and heat balance inside the electrode. A simplified bondgraph representation [4] of this approach is presented in Fig. 4.

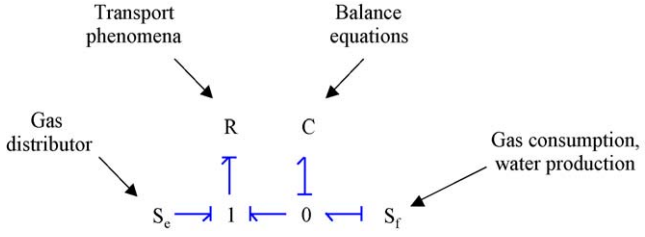

Fig. 4. Hydraulic model of the electrode.

3.3.1. Transport phenomena

The diffusion fluxes in the gas phase are driven by the inverted Stefan–Maxwell equations (3)–(5). The molar fluxes F_i are computed from the molar fraction difference ΔX_i, taking into account the thickness e and the surface S of the electrode, the molar masses M_i of the species, the gas concentration C_{g} and the gas density ρ_{g} [9].

$$\frac{F_x}{S} = \frac{C_{\text{g}}^2}{\rho_{\text{g}}}\left(M_v D_{xv}^{\text{T}}\frac{\Delta X_v}{e} + M_n D_{xn}^{\text{T}}\frac{\Delta X_n}{e}\right) \tag{3}$$

$$\frac{F_n}{S} = \frac{C_{\text{g}}^2}{\rho_{\text{g}}}\left(M_v D_{nv}^{\text{T}}\frac{\Delta X_v}{e} + M_x D_{nx}^{\text{T}}\frac{\Delta X_x}{e}\right) \tag{4}$$

$$\frac{F_v}{S} = \frac{C_{\text{g}}^2}{\rho_{\text{g}}}\left(M_n D_{vn}^{\text{T}}\frac{\Delta X_n}{e} + M_x D_{vx}^{\text{T}}\frac{\Delta X_x}{e}\right) \tag{5}$$

The diffusion coefficients D_{ij}^{T} in a ternary (three species) mixture used in these equations are deduced from the binary diffusion coefficients D_{ij}, considering the molar fraction x_i and the molar mass M_i of each species.

$$D_{ij}^{\text{T}} = D_{ij}\left[1 + \frac{x_k\left(\frac{M_k}{M_j}D_{ik} - D_{ij}\right)}{x_i D_{jk} + x_j D_{ik} + x_k D_{ij}}\right] \tag{6}$$

The coefficients D_{ij} used in the porous electrodes are corrected from their nominal values D_{ij} [1,3] to take into account porosity ε of the material and liquid water saturation s.

$$D_{ij} = [(1-s)\varepsilon]^{3/2} D_{ij} \tag{7}$$

These equations are completed by convective transport terms for gas and liquid phases (8), (9).

$$\frac{F_{\text{g}}}{S} = \frac{KK_{\text{rg}}(s)}{M_{\text{g}}\nu_{\text{g}}}\frac{\Delta P_{\text{g}}}{e} \tag{8}$$

$$\frac{F_{\text{l}}}{S} = \frac{KK_{\text{rl}}(s)}{M_{\text{l}}\nu_{\text{l}}}\frac{\Delta P_{\text{l}}}{e} \tag{9}$$

where $K_{\text{rg}}(s) = (1-s)^3$ and $K_{\text{rl}}(s) = s^3$ are the relative permeabilities.

3.3.2. Balance equations

The model computes the mass balance (10)–(13) for each component (written here for the cathode side):

$$\frac{\text{d}n_{\text{O}_2}}{\text{d}t} = \sum F_{\text{O}_2} \tag{10}$$

$$\frac{\text{d}n_{\text{N}_2}}{\text{d}t} = \sum F_{\text{N}_2} \tag{11}$$

$$\frac{\text{d}n_{\text{vap}}}{\text{d}t} = \sum F_{\text{vap}} - F_{\text{v}\to\text{l}} \tag{12}$$

$$\frac{\text{d}n_{\text{liq}}}{\text{d}t} = \sum F_{\text{liq}} + F_{\text{v}\to\text{l}} \tag{13}$$

where n_{spc} is a number of moles of the specie spc, $\sum F_{\text{spc}}$ the algebraic sum of the inlet and outlet fluxes for this specie, $F_{\text{v}\to\text{l}}$

is the algebraic rate of condensation for the water (negative if water evaporates).

Vapor saturation is then calculated (14), (15) and rates of evaporation or condensation necessary to stay close to the liquid/vapor equilibrium are estimated (16), (17).

$$X_{\text{sat}} = \frac{P_{\text{sat}}(T)}{P} \tag{14}$$

$$X_{\text{vap}} = \frac{n_{\text{vap}}}{n_{\text{vap}} + n_{\text{O}_2} + n_{\text{N}_2}} \tag{15}$$

If $n_{\text{liq}} > 0$ or $hA(X_{\text{vap}} - X_{\text{sat}}) + \sum F_{\text{liq}} > 0$

$$F_{\text{v}\to\text{l}} = hA(X_{\text{vap}} - X_{\text{sat}}) \tag{16}$$

else

$$F_{\text{v}\to\text{l}} = -\sum F_{\text{liq}} \tag{17}$$

Gas and liquid pressures are then deduced, considering the volume occupied by liquid water (18), (19), using the perfect gas hypothesis and considering capillary effect for water pressure calculation (19)–(22).

$$V_{\text{liq}} = \frac{n_{\text{liq}} M_{\text{liq}}}{\rho_{\text{liq}}} \tag{18}$$

$$V_{\text{gaz}} = V - V_{\text{liq}} \tag{19}$$

$$P_{\text{gaz}} = \frac{(n_{\text{O}_2} + n_{\text{N}_2} + n_{\text{vap}})RT}{V_{\text{gaz}}} \tag{20}$$

$$P_{\text{cap}} = \frac{\sqrt{8}}{R_{\text{p}}}\sigma\cos(\theta)J(s) \tag{21}$$

$$P_{\text{liq}} = P_{\text{gaz}} - P_{\text{cap}} \tag{22}$$

where $J(s)$ is the so known Leverett function [10], R_{p} the pores sizes, σ the superficial tension and θ contact angle.

At last, the energy balance equation is used to compute the temperature in each mesh (23):

$$\begin{aligned}(n_{\text{O}_2}C_{p_{\text{O}_2}} + n_{\text{N}_2}C_{p_{\text{N}_2}} + n_{\text{liq}}C_{p_{\text{liq}}} + n_{\text{vap}}C_{p_{\text{vap}}})\frac{\text{d}T}{\text{d}t} \\ = \sum F_{\text{O}_2}C_{p_{\text{O}_2}}(T_{\text{e}} - T) + \sum F_{\text{N}_2}C_{p_{\text{N}_2}}(T_{\text{e}} - T) \\ + \sum F_{\text{liq}}C_{p_{\text{liq}}}(T_e - T) \\ + \sum F_{\text{vap}}C_{p_{\text{vap}}}(T_{\text{e}} - T) + F_{\text{v}\to\text{l}}L_{\text{v}}(T) + V\frac{\text{d}P}{\text{d}t} + Q\end{aligned} \tag{23}$$

where T_{e} is the inlet temperature for each component and T the mixture temperature inside the electrode. C_p is the thermal capacity and L_{v} the latent heat for water evaporation. The contribution $V\frac{\text{d}P}{\text{d}t}$ related to adiabatic compression is usually neglected because we do not study very sharp pressure transients.

3.4. Membrane

The model of the membrane considers two meshes for mass transport, anode and cathode sides (Fig. 5), and one mesh for mass balance. The water content of the electrolyte is computed dynamically from the interfacial conditions.

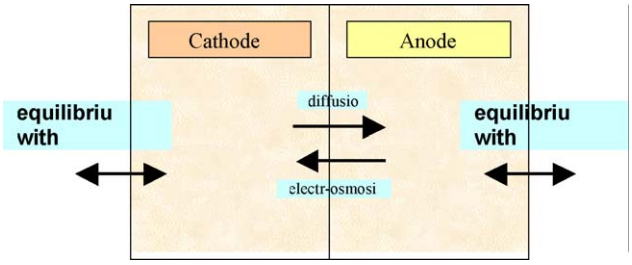

Fig. 5. Model of water transport in the membrane.

Equilibriums with hydration conditions in the electrodes are given [3,5] for anode and cathode side by (24).

$$\lambda = \begin{cases} \text{if } a \le 1 \quad \text{then } 0.043 + 17.81a - 39.85a^2 + 36.0a^3 \\ \qquad\qquad \text{else } 14 + 1.4(a-1) \end{cases} \tag{24}$$

where a is the water activity in the electrode at the interface with the membrane and λ is the water content of the membrane at the interface with the electrode. The diffusion coefficient for each mesh is then estimated [3] using (25)

$$D_\lambda = (6.707 \times 10^{-8}\lambda + 6.387 \times 10^{-7}) \exp\left(-\frac{2416}{T}\right) \tag{25}$$

and the diffusion flux through the mesh is computed using (26)

$$\frac{F_{\text{diff}}}{S} = \frac{\rho_{\text{sec}}}{EW} D_\lambda \frac{(\lambda_c - \lambda_a)}{e_{\text{m}}} \tag{26}$$

where F_{diff} is the flux of diffusion (mol s^{-1}) and e_{m} is the thickness of the half membrane. In a same way, the electro-osmosis flux is given [3] by (27)

$$F_{\text{eo}} = \frac{a_{\text{eo}}\, I}{2F} \tag{27}$$

where F_{eo} is the molar flux, I is the current and F is the Faraday constant.

3.5. Electrochemical response

The relations giving the thermodynamic potential and the activation over-voltage can be found in [1] and [2]. Global cell potential (for one mesh) is given by (28).

$$U = E_{\text{rev}} + \eta_{\text{act}} - R_{\text{m}} I \tag{28}$$

where

$$E_{\text{rev}} = \alpha_1 + \alpha_2(T - 298.15) + \alpha_3 T(0.5 \ln P_{\text{O}_2} + \ln P_{\text{H}_2}) \tag{29}$$

is the thermodynamic potential and

$$\eta_{\text{act}} = \beta_1 + \beta_2 T + \beta_3 T \ln i + \beta_4 T \ln P_{\text{O}_2} \tag{30}$$

is the activation over-voltage. The temperature T and the partial pressures P_{O_2}, P_{H_2} are the local conditions at the active layers of the electrodes. The coefficients α_i are calculated from physical parameters [1,2]. The coefficients β_i are fitted to experimental

results (Section 4). R_m is the membrane electrical resistance. The local current density i depends on the amount of liquid water in the electrode according to (31)

$$i = \frac{I}{1-s} \tag{31}$$

where I is the surface current density and s the volume ratio of liquid water in the electrode (s can theoretically vary from 0 to 1, simulations have given typical values of 0.2 in usual conditions).

At last, the superficial heat production is given [1] by (32).

$$\frac{Q}{S} = (1.2517 - U)I \tag{32}$$

By convention in this model, the heat production is calculated using the lower heating value (LHV), i.e. considering a vapor water production (possible condensation that depends on local temperature and pressure conditions is considered in another part of the model). The LHV is computed for the standard conditions (the variation with the temperature or with the pressure is lower than 1% in our range of conditions [1]).

4. Parameters estimation

The parameters that have to be identified are the coefficients of the local electrochemical response. To be able to identify these parameters, it is necessary to vary current density, gases' partial pressure, and temperature. One difficulty is that the independent variables involved in the model are different from those controlled in the experiment: the experimental setup does not allow to directly impose the local conditions, but they have to be computed starting from measured parameters (plate temperature, pressure in the gas distributors, inlet gas composition) and using the model. So the method for model identification is iterative: at first, we compute local conditions using parameters from the literature [1,2] for electrochemical response. Using these computed conditions (hydrogen and oxygen partial pressures, local current density and membrane resistance) we are able to fit the parameters of (30). We can then compute again the local conditions, using the updated set of parameters. These steps are iterated until the parameters do not change any more from one iteration to another. In fact, the computed local conditions were found not to be very sensitive to the electrochemical response, and usually two iterations were enough to achieve identification.

The parameters fitting is performed using Matlab©'s linear regression capabilities. Considering (30) we define:

$$x_1 = T, \qquad x_2 = T\log(i), \qquad x_3 = T\log(P_{O_2}), \quad \text{and}$$
$$X = [\ 1 \quad x_1 \quad x_2 \quad x_3\ ] \tag{33}$$

(where x_i is a vector in which number of elements corresponds to the number of experiments to simulate) to obtain a linear relation (34). If y is the measured overvoltage, the coefficients $b = [\ \beta_1 \quad \beta_2 \quad \beta_3 \quad \beta_4\ ]$ of (30) can be fitted by linear regression of the model (34).

$$y = Xb \tag{34}$$

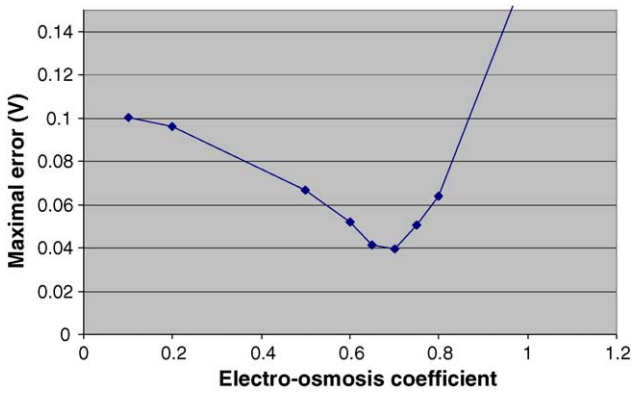

Fig. 6. Maximal error between experiment and simulation for varying electro-osmosis coefficient.

A total of 36 experimental runs, covering the most working conditions, are used for this identification. As the model of cell is meshed into 10 parts from inlet to outlet, each vector x_i is composed of 360 values. The values of the parameters found are (35):

$$\beta_1 = -8.25 \times 10^{-1}, \qquad \beta_2 = 1.87 \times 10^{-3},$$
$$\beta_3 = -2.16 \times 10^{-4}, \qquad \beta_4 = 8.75 \times 10^{-5} \tag{35}$$

Another iteration level was necessary to find out the optimal value (the one that allows the best fit for the other parameters) of the electro-osmosis coefficient used in (27) (Fig. 6).

In a second phase, experimental data obtained with air (with a stoichiometric ratio fixed to 2) allowed to fit the porosity of the electrodes, influencing diffusion coefficients used in (3)–(5). The parameters of the electrochemical response were of course kept unchanged. A porosity of 0.15 was found for the electrodes. This value is low compared to porosities usually found in literature [3,5], but we can note that the porosity is related to the thickness of the electrodes, that is unknown.

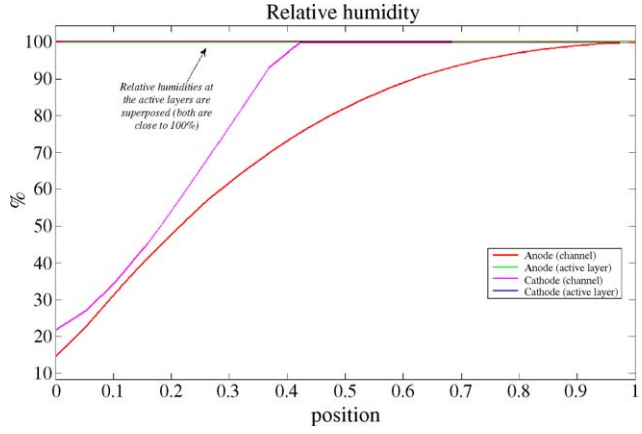

Fig. 7. Relative humidity in the channels and inside the electrodes at 70 °C and 2.5 bar, working with dry H_2 and air. Position 0 is the inlet of the stack, position 1 is the outlet.

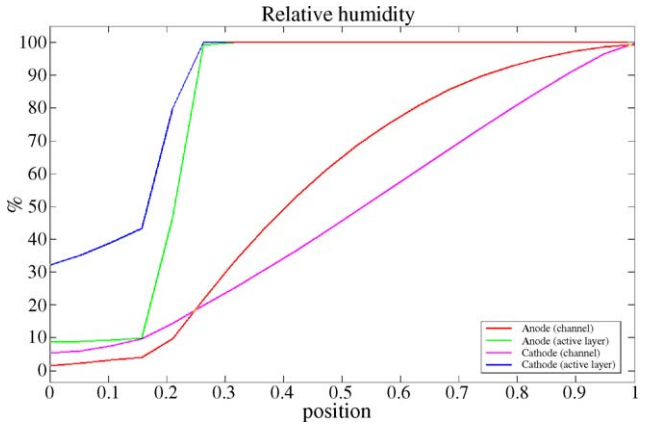

Fig. 8. Relative humidity in the channels and inside the electrodes at 80 °C and 2.0 bar, working with dry H_2 and air. Position 0 is the inlet of the stack, position 1 is the outlet.

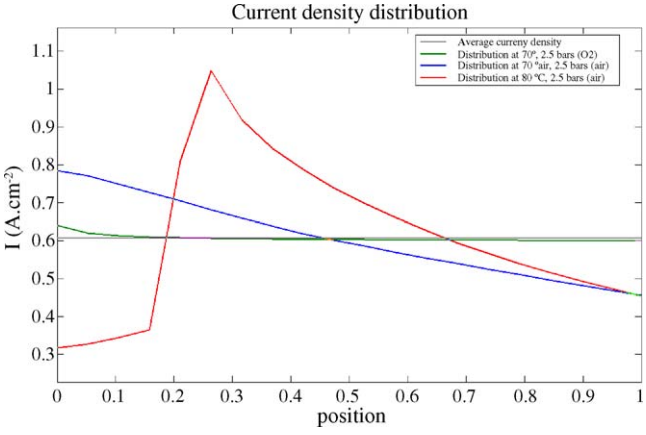

Fig. 9. Current distributions in the stack for different conditions (dry gases). Position 0 is to the inlet of the stack, position 1 is the outlet.

5. Stack operation characterization

As the model is fitted, we can perform simulations in order to access local gas composition and current distribution. The simulations show that for the stack working with air at 2.5 bar absolute pressure, the membrane will not dry out. This can be explained by Fig. 7, the vapor diffusion through the gas diffusion layer limits the water transfer. Consequently, the current density is homogeneous along the surface of the cells, and no effect on the cell voltage is expected.

If we decrease the working pressure down to 2.0 while increasing the temperature up to 80 °C, simulations predict a drying out of the membrane and active layers at the stack inlet as shown in Fig. 8. This leads to inhomogeneous current distributions along the cell, as illustrated in Fig. 9.

These simulations are confirmed by experimental results: an effect of gas hydration on stack voltage was in fact observed at 2.0 bars and 80 °C, whereas no effect was noticed at 2.5 bars.

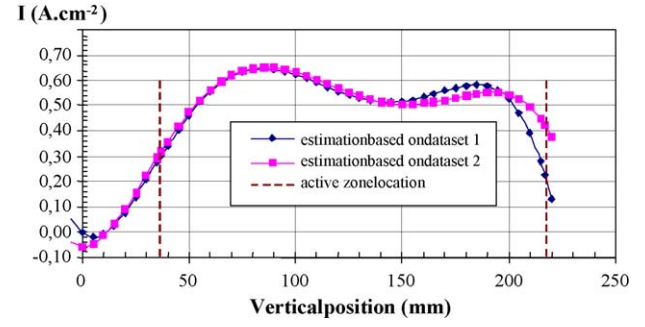

Fig. 10. Experimental current distribution for H_2/O_2 gas feeding. Two experimental runs are compared.

6. Conclusion

We have developed a model that allows to access internal operation of the stack. This model was successfully fitted on experimental data obtained on a test bench in the context of the PICOS project. The fitted model is able to compute the one-dimensional current density profile in the stack and to reproduce effects of temperature, pressure and gas humidification on the stack voltage. Effects of low gas humidification and resulting drying out of the membrane (depending on stoichiometric ratios, pressure and temperature) can be predicted. Experimental devices allowing to perform a measurement of current densities (based on magnetic field) are currently under development in order to confirm the predictions of the model.

First tests in O_2/H_2 gas alimentation are promising (Fig. 10), the measured current density is in accordance with the total current. As expected under these conditions, the current distribution obtained is nearly uniform. These results can be compared to simulation results (Fig. 9). The differences may be attributed to mechanical constraints in the stack and border effects that are so far not taken into account in the model.

Acknowledgments

This work was achieved within the context of the PICOS project (2001–2003) aiming at the development of a PEMFC prototype for submarine applications. PICOS was labellised by the French Research and Technical Innovation Network on fuel cells (RIT PACo) and supported by the French Ministry of Economy, Finances and Industry (MEFI). PICOS was completed in partnership by IFREMER, ECA, SORAPEC and CEA-Grenoble. The model was partly built in the project SPACT, involving INRETS, UTBM and CEA-Grenoble and supported by French Ministry of Research.

References

[1] J.P. Poirot-Crouvezier, Modélisation dynamique des phénomènes hydrauliques, thermiques et électriques dans un groupe électrogène à pile à combustible, PhD, INPG, 2000.

[2] J.C. Amphlett, R.M. Baumert, R.F. Mann, B.A. Peppley, P.R. Roberge, T.J. Harris, Performance modeling of the Ballard mark IV solid polymer electrolyte fuel cell, I. Mechanistic model development, J. Electrochem. Soc. 142 (1995) 1–8.

[3] L. Gerbaux, Modélisation d'une pile à combustible de type hydrogène/air et validation expérimentale, PhD, INPG, 1996.
[4] D.C. Karnopp, D.L. Margolis, R.C. Rosenberg, System Dynamics: A Unified Approach, 2nd ed., John Wiley & Sons, New York, USA, 1990.
[5] T.E. Springer, T.A. Zawodzinski, S. Gottesfeld, Polymer electrolyte fuel cell model, J. Electrochem. Soc. 138 (8) (1991) 2334.
[6] P. Schott, J.-P. Poirot, P. Baurens, Modélisation et simulation de la source d'énergie à pile à combustible du véhicule Hydro-Gen, Ann. Chim. Sci. Mat. 26 (4) (2001) 27–42.
[7] J. Lachaize, M. Fadel, S. Caux, P. Schott, L. Nicod, Modelling and control of a fuel cell system in transport application, in: IFAC 2003, Shanghai, PR China, Octobre 11–13, 2003.
[8] G. Dauphin-Tanguy, Les bondgraphs, éditions Hermès, 2000.
[9] R.B. Bird, W.E. Stewart, E.N. Lightfoot, Transport Phenomena, Wiley International Edition, 1960.
[10] C.Y. Wang, C. Beckermann, A two phase mixture model of liquid–gas flow in capillary porous media, Int. J. Heat Mass Transfer 36 (11) (1993) 2747–2758.